Self-Healing Materials with Interpenetrating Microvascular Networks

By *Christopher J. Hansen, Willie Wu, Kathleen S. Toohey, Nancy R. Sottos,* Scott R. White,* and *Jennifer A. Lewis**

Complex microvascular networks are widely observed in biological systems, such as leaf venation[1–4] and blood vascularization.[5–7] These networks enable targeted delivery of nutrients for growth and healing. Due to their complicated architecture, replication of these microvascular systems remains a significant challenge for those pursuing synthetic analogs. Various techniques, including soft lithography,[8–10] laser ablation[11,12] and direct-write assembly[13] have been employed to create planar and 3D microvascular networks. However, to date, simple networks composed of single, uniform vascular pathways have mainly been constructed.

Of particular interest is the ability of microvascular networks to enable repetitive healing of damage in biological and synthetic systems. For example, human skin can undergo repeated repair of damage in a single location (Fig. 1a). The outer layer of skin (the epidermis) serves as a protective coating, preventing outside pathogens from infiltrating the body.[15] The dermis, which lies beneath this layer, contains a complicated microvascular network composed of larger blood vessels that branch into smaller capillaries, which deliver nutrients to and remove waste products from the dermal and epidermal regions. Two similar, yet distinct, microvascular networks accomplish these functions. Replication of biological self-healing in structural materials that suffer repeated mechanical damage could dramatically increase service lifetimes.[16–19]

Toohey et al.[14] recently reported a new self-healing architecture that mimics human skin, based on a epoxy coating/substrate architecture, in which a microvascular network is embedded by direct-write assembly of a fugitive organic ink.[13,20] When a crack is formed in the coating due to mechanical damage, the microvascular network in the underlying substrate supplies a healing agent, dicyclopentadiene (DCPD), to the crack plane, where it comes into contact with Grubbs' catalyst contained within the coating. Unlike earlier work in which self-healing was

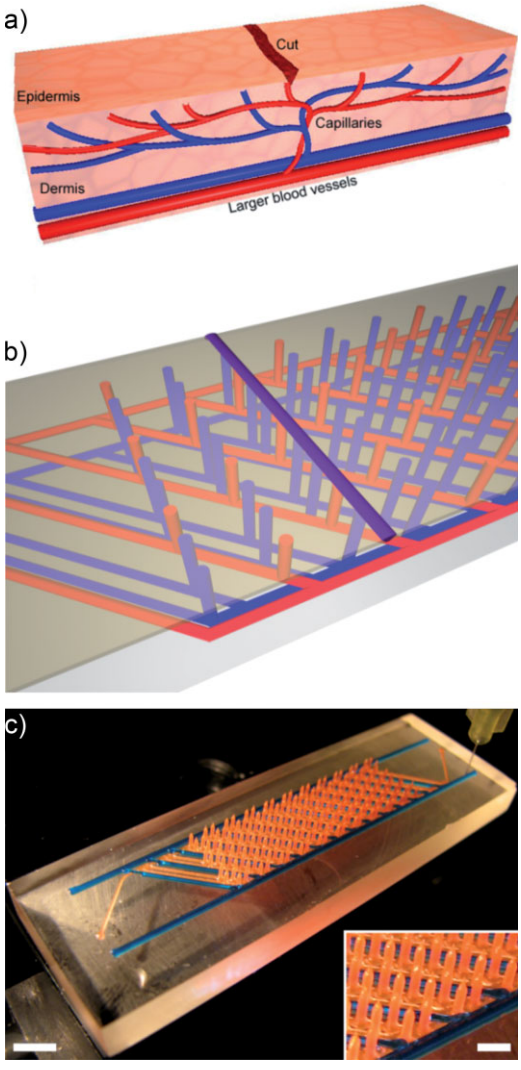

Figure 1. a) Schematic view of a cut in the epidermis layer of skin and the capillary network in the dermis layer. b) Schematic view of an interpenetrating microvascular network that supplies two fluids (red and blue) to a crack plane, where mixing occurs (purple). c) Interpenetrating microvascular network fabricated by direct-write assembly of wax (orange)- and pluronic (blue)-based fugitive inks. Scale bar = 5 mm. Inset: magnified view of vertical features printed from wax-based ink. Scale bar = 1 mm. Figure 1a reproduced with permission from [14]. Copyright 2007 Nature Publishing Group.

[*] Prof. N. R. Sottos, Prof. J. A. Lewis, C. J. Hansen, W. Wu, K. S. Toohey, Prof. S. R. White
Autonomic Materials Systems Group
Beckman Institute for Advanced Science and Technology
University of Illinois at Urbana-Champaign
Urbana, IL 61801 (USA)
E-mail: n-sottos@illinois.edu; jalewis@illinois.edu
Prof. N. R. Sottos, Prof. J. A. Lewis, C. J. Hansen, W. Wu
Department of Materials Science and Engineering
University of Illinois at Urbana-Champaign
Urbana, IL 61801 (USA)
Prof. S. R. White
Department of Aerospace Engineering
University of Illinois at Urbana-Champaign
Urbana, IL 61801 (USA)

DOI: 10.1002/adma.200900588

confined to a single event in a given localized region,[21] this first-generation biomimetic design enabled repeated healing up to seven cycles. However, beyond this point, healing ceases due to depletion of catalyst in the crack plane. To overcome this limitation, Toohey et al. recently modified this design by photolithographically patterning four isolated regions within the embedded microvascular network.[22] Specifically, the interconnected network was filled with a photopolymerizable resin that was locally cured to produce a solid barrier between isolated regions within the network. After the remaining unpolymerized resin was removed, each isolated network region was filled with alternating components of a two-part healing chemistry composed of epoxy resin and hardener. This modified design not only allows new healing chemistries to be explored, but ensures that neither healing agent is depleted. In this work, up to 16 intermittent healing events out of 23 cycles were achieved. A key disadvantage of this approach is that healing agents must migrate and diffusively mix over long distances within the crack plane, which correspond roughly to the half thickness of a given isolated microvascular region. Importantly, even these simple networks, which do not obey Murray's law, greatly enhance the performance of self-healing materials.

In a related effort, Williams et al. have demonstrated self-healing in sandwich composite configurations that contain either single[23] or dual[24] fluidic networks. In the single network design, premixed epoxy resin and hardener are introduced into 1.5 mm channels leading to full mechanical recovery during a single cycle.[23] In their dual network design, significant recovery is observed when samples are infiltrated with pressurized unmixed fluids.[24]

Here, we demonstrate a new biomimetic coating/substrate architecture design, in which a three-dimensional interpenetrating microvascular network is embedded to enable repeated, autonomous healing of mechanical damage (see Fig. 1b). To fabricate the interpenetrating microvascular network shown in Figure 1c, two key advances in direct-write assembly are required: i) dual ink deposition and ii) vertical ink writing. We first independently deposit two fugitive organic inks to construct the desired interpenetrating, yet isolated, microvascular networks. Next, we pattern vertical posts that connect each underlying network, embedded within the epoxy substrate, to the coating, thereby providing conduits that supply both healing agents to the crack plane when damage occurs. To facilitate direct-write assembly, both inks must flow through a fine deposition nozzle under high shear, and form self-supporting filaments upon exiting the nozzle. Furthermore, to maintain network isolation, both inks must be removed independently from the epoxy substrate. To meet these challenging demands, we created two fugitive organic inks that possess similar viscoelastic behavior under ambient (printing) conditions, yet have vastly different temperature-dependent rheological responses.

The primary fugitive ink is composed of a mixture of microcrystalline wax and mineral oil, which represents a modified form of the wax-based ink reported previously.[20,25] Under ambient conditions, this ink exhibits a plateau shear elastic modulus, G', of 10^5 Pa, and pronounced shear thinning when the applied stress exceeds the shear yield stress, τ_y (Fig. 2a). When the temperature is raised to 50 °C, both the plateau G' and τ_y are significantly reduced. Above approximately 80 °C, the ink liquefies and can be removed from the epoxy matrix under a light vacuum, leaving behind the desired microchannels.

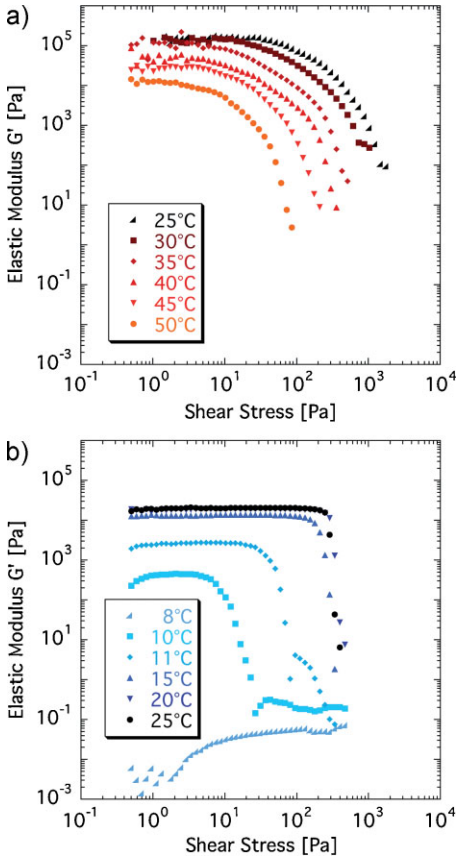

Figure 2. Log–log plots of shear elastic modulus as a function of applied shear stress for a) wax- and b) pluronic-based fugitive inks at varying temperatures.

The secondary fugitive ink is composed of an aqueous, triblock-copolymer solution. The triblock copolymer, known as Pluronic F127, consists of poly(propylene oxide) (PPO) and poly(ethylene oxide) (PEO) arranged in an ABA configuration of $PEO_{106}PPO_{70}PEO_{106}$, with an average molecular weight of approximately 12,600.[26] The copolymer species assemble into micelles at temperatures above ≈10 °C, yielding a physical gel when the copolymer concentrations exceeds ≈20 w/w%.[27–30] For a copolymer concentration of 30 w/w%, a plateau G' of approximately 10^4 Pa is observed under ambient conditions (Fig. 2b). However, unlike the wax-based ink, this copolymer ink softens as the temperature is decreased (Fig. 2b). Importantly, below the micellization temperature, this secondary fugitive ink becomes fully liquefied, such that the plateau G' is reduced by six orders of magnitude at 8 °C.[28]

The interpenetrating microvascular network design in Figure 1c requires both dual and vertical ink writing (see Supporting Information, Fig. S1). In this approach, the primary and secondary fugitive inks are mounted side-by-side on a 3D robotic deposition stage, such that each ink is patterned independently (Supporting Information, Movie S1). The primary fugitive ink is used to define both interpenetrating microvascular

networks as well as the vertical conduits, while the secondary fugitive ink serves to separate each network so they remain isolated in the final coating/substrate architecture. To produce the vertical conduits shown in Figure 1c, the ink is deposited through a 330 μm nozzle, as it translates along the z axis (see Supporting Information, Movie S2). Ink flow is started and stopped repeatedly to create up to 420 vertical features per specimen.

Vertical ink writing depends critically on the ink elasticity, nozzle diameter (D), and filament height (h). To determine the aspect ratios (h/D) achievable from the primary fugitive ink, we printed vertical features of varying height through a wide range of nozzle diameters (Fig. 3). We find that stable vertical features with $h/D \approx 25$–35 can be produced using nozzles that range from 500 μm to 100 μm in diameter, respectively. As the value of h/D is further increased, the vertical filaments first undergo buckling followed by complete collapse.[31–33] For the self-healing specimens studied, vertical filaments with a $h/D \approx 15$ were patterned using a 300 μm nozzle.

To create the desired self-healing specimens, we first fill the void space between patterned ink filaments with a low-viscosity epoxy resin.[13,14,20] Next, we remove the secondary fugitive ink from the epoxy substrate by cooling the specimen to ≈5 °C. The resulting microchannels are then infiltrated with the epoxy resin and the specimen is again cured. The primary fugitive ink, whose pattern defines the two interpenetrating microvascular networks, remains within the substrate, but is now fully surrounded by the epoxy matrix. Finally, upon heating the specimen to ≈80 °C, the primary fugitive ink is liquefied and removed to yield the desired interpenetrating, yet isolated, microvascular networks (see Supporting Information, Fig. S1).

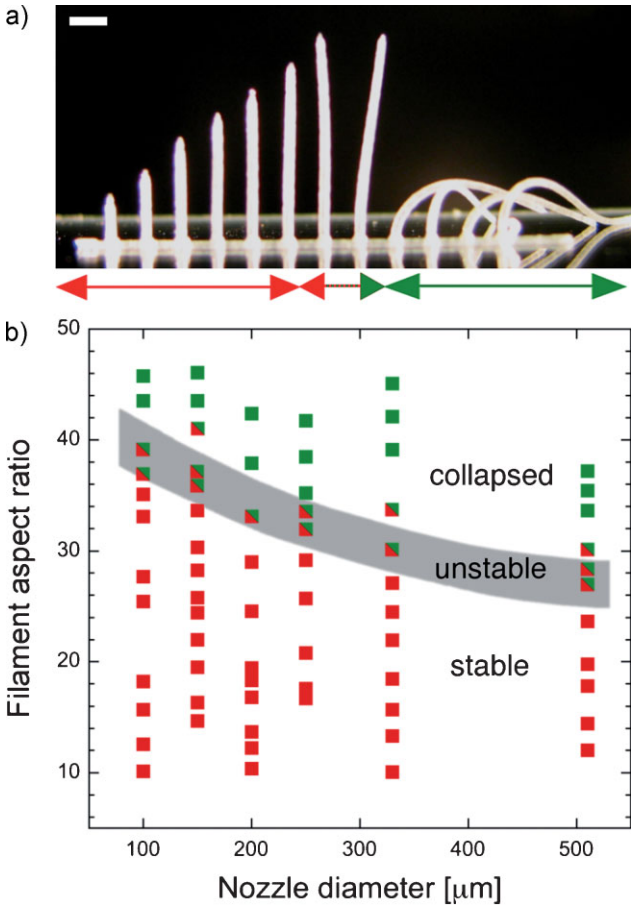

Figure 3. a) Optical image of printed vertical features with varying aspect ratios that demonstrate the transition from stable to buckled form. Scale bar = 1 mm. b) Stability map of printed vertical features. Stable features (red squares) become unstable at increasing aspect ratios (red/green squares), finally collapsing at yet higher aspect ratios (green squares).

To investigate autonomic healing of coating/substrate architectures with interpenetrating microvascular architectures, we fill each network with one component of a two-part epoxy chemistry. Specifically, one network is filled with the epoxy resin, while the second network is filled with epoxy hardener. Because the networks are isolated from one another within the substrate, these fluids will only react when they come in contact within the crack plane of the coating layer. Eight specimens are produced, each of which contains vertical posts that deliver a 2:1 ratio of resin:hardener, approximating the optimal stoichiometry (2.2:1).[24] Prior to mechanical testing, the crack location is specifically defined by producing a horizontal line on the coating surface using a scribe tool under constant load, which is placed above an array of vertical posts beneath the coating. Following the procedure reported previously,[14] each specimen is then placed in a four-point bend geometry and loaded until the coating fractures. There is a small (10%) difference between the critical loads observed for specimens that have been scored ((114 ± 23) N) versus unscored ((129 ± 57) N). Scoring the specimen surface increases repeatability and produces a single straight crack that propagates through the coating to the coating/substrate interface, yet does not proceed into the underlying substrate. Once the crack reaches this interface and contacts the interpenetrating microvascular network, both epoxy resin and hardener wick into the crack plane due to capillary forces. The specimens are then subject to cyclic flexure loading (50 cycles at 100 μm displacement) to enhance mixing of the fluids in the crack plane prior to healing at 30 °C for 48 h. After healing, each specimen is tested again, and the original crack reopens at a new critical load. This process is repeated for 30 cycles. The load curves for the original crack and after 30 subsequent heal cycles are shown for one representative specimen in Figure 4a. This specimen demonstrates the remarkable ability of interpenetrating microvascular networks to enable repeated healing of a single crack for 30 sequential cycles. Healing was tested for eight specimens for 30 consecutive cycles, for a total of 240 cycles. Of these cycles, there was no detectable acoustic emission event in nearly 33% of the cycles, and these specimens were considered to have not healed for that cycle. The fraction of nonhealing cycles increased with increasing number of healing cycles, rising from an average of 0.25 initially to 0.46 for the last three cycles (see Fig. 4b). Similar to previously reported results,[22] we observe no increase in the healing loads with mixing, but rather an increase in the number of consecutive healing cycles.

The healing efficiency, η, is defined as the ratio of fracture toughness of the coating for a specific heal cycle to the original fracture toughness. For the specimen geometry used in this study, the healing efficiency simplifies to a ratio of the heal fracture load to the original fracture load, calculated as $\eta = P^{Healed}/P^{Original}$. The average healing efficiency for the eight specimens tested is

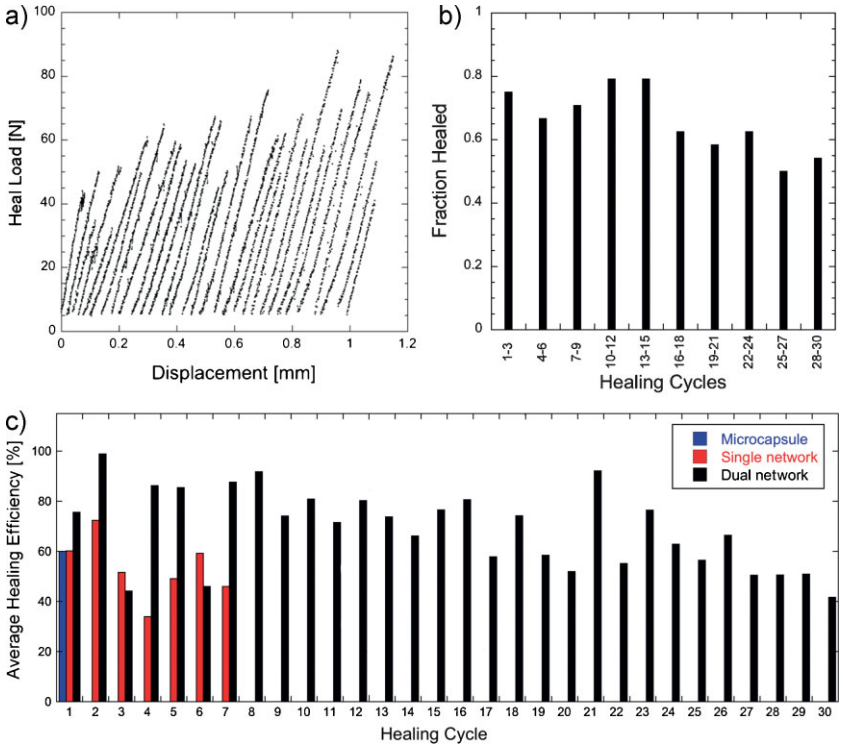

Figure 4. a) Load-displacement curves for one specimen exhibiting over 30 continuous healing cycles, where the first curve denotes the original fracture. b) Fraction of specimens (out of eight total) demonstrating healing per cycle. c) Average healing efficiency for these specimens over 30 heal cycles, compared with prior data from microcapsule (blue) [21] and single-network microvascular (red) [14] systems.

provided in Figure 4c. Nonhealed samples were assigned a value of $\eta = 0$ and were averaged with the healed samples in each test cycle. The value of η approaches 100% in some cases, and a healing efficiency of ≈50% is retained after 30 cycles of healing. This compares favorably with the previous self-healing microcapsule and single-network geometries, also shown in Figure 4c. The interpenetrating network specimens show healing efficiency comparable to that of the microcapsule specimen for the initial healing cycle, demonstrating no sacrifice in healing efficiency due to the new geometry. For the first seven cycles, the interpenetrating network matches or exceeds the healing efficiency of the single-network geometry, again showing no sacrifice in healing efficiency with the new design. Finally, the total number of observed healing cycles is unparalleled, demonstrating the superiority of this new interpenetrating microvascular network design.

In summary, we have demonstrated the ability to create autonomic materials with interpenetrating microvascular networks that independently supply multiple healing agents to a given damage site. These novel coating/substrate architectures were created through two key advancements in direct-write assembly – dual and vertical ink writing. This platform enables not only the use of new healing chemistries, such as a two-part epoxy system, but also repeated healing over tens of mechanical testing cycles.

Experimental

Fugitive Inks: Microcrystalline wax ink is prepared by the addition of 60 w/w% microcrystalline wax (SP-19, Strahl & Pitsch, Inc.) and 40 w/w% heavy mineral oil (Fischer Scientific). The components are melted at approximately 100 °C and stirred for 10 min. The melted solution is poured into 3 mL syringes (EFD Inc.) and placed in a 70 °C oven until the ink solidifies, after which the syringe is cooled to room temperature. The triblock-copolymer ink is prepared with 30 w/w% polymer (Pluronic F128, BASF) in deionized water. The copolymer is slowly stirred into an aqueous solution held at 5 °C. After the copolymer is fully dissolved, the solution is refrigerated for at least 12 h to remove all air bubbles. The cooled solution is poured into 3 mL syringes and then warmed to ambient temperature.

Ink Rheology: The storage shear modulus, G', is measured using a controlled-stress rheometer (CVOR-200, Bohlin) fitted with a cone and plate geometry. An appropriate amount (<1 mL) of ink is placed in the geometry, which is maintained at the desired temperature using a circulating bath (Model 9110, Polyscience). The wax ink is initially held at 25 °C and increased in 5 °C increments, while the pluronic ink is initially held at 5 °C and increased in temperature between tests. Oscillatory-shear measurements are carried out at 1 Hz by incrementally increasing the stress amplitude from 0.5 to 2000 Pa for the wax ink and from 0.1 to 1000 Pa for the pluronic ink.

Vertical Printing: To create vertical features, the nozzle is positioned over a desired location and pressure is applied to initiate ink deposition. The nozzle position is maintained until ink deposition commences (usually ≈0.2 s), after which the nozzle is raised at a rate equal to the deposition rate. After the desired feature height is achieved, ink deposition is stopped by reducing the applied pressure to zero; concomitantly, the nozzle is lifted vertically until the deposited-ink features is disconnected from the nozzle. After deposition of vertical features through nozzles ranging in diameter from 100 to 410 μm, optical images are taken with a digital camera (PowerShot S2 IS, Canon). The filament diameter, aspect ratio, and stability are determined using image-processing software ImageJ (NIH).

Microvascular Substrate Fabrication: Microvascular interpenetrating networks are fabricated using a three-axis robotic deposition stage (ABL9000, Aerotech Inc.) whose motion is controlled by customized software (RoboCAD version 3.1). Wax and pluronic inks are housed in syringes that are fitted with 330 and 100 μm nozzles (EFD Inc.), respectively. The syringes are mounted side-by-side in air-pressure multiplier dispensing systems (HP7X, EFD Inc.). Each ink is extruded at a rate of 4 mm s^{-1} onto precured epoxy substrates (Envirotex Lite, Environmental Technologies Inc.). The wax ink is patterned first, followed by the pluronic ink, which serves as a supporting layer for further ink deposition. This process is repeated as needed to construct the desired interpenetrating microvascular network. Upon completion, the patterned structures are infiltrated with the same epoxy matrix material as the substrate and cured for 24 h at 20 °C. Specimens are cut to allow access to the embedded pluronic ink, which is removed via dissolution in water. Upon completely removing the pluronic ink, the specimens are dried and reinfiltrated with the epoxy matrix materials and allowed to cure. The specimens are cut and polished to final dimensions (50 mm × 12 mm × 6 mm), then heated to 80 °C to melt the wax ink, which is removed upon the application of a light vacuum. Any residual ink is removed via ultrasonication for 5 min with a 20 w/w% aqueous degreaser solution (VCPI-411, Cortec).

Coating Application: A fugitive wax (Purester 24, Strahl & Pitsch) is infiltrated in the surface posts to prevent the uncured coating mixture from infiltrating the microvascular network. The coating, a mixture of 12 p.p.h. diethylenetriamine (Air Products Inc.) in EPON 828 resin (Miller Stephenson Inc.), is degassed for 30 min and applied to the substrate surface. The coating is cured for 6 h at 25 °C, followed by 9 h at 30 °C. The coating is polished to a final thickness (≈700 μm), and the fugitive wax is removed by heating to 35 °C and applying a light vacuum.

Fracture Testing and Healing Efficiency: The specimen is filled with epoxy resin (EPON 8132, Miller-Stephenson) in one network and with epoxy hardener (Epikure 3046, Miller-Stephenson) in the other network. The specimen coating is notched ≈5–10 μm in depth, as measured by an optical profilometer (CHR-150, STIL), by a scribe under constant load (6–10 N) using a test panel scratcher (Corrocutter 639, Erichsen). This notch is specifically located above a row of network spikes (Supporting Information, Fig. S2a). The specimen is loaded in four-point bending, as previously reported [14] (Supporting Information, Fig. S2b), and load–time data are collected using LabVIEW software (v6.5, National Instruments). An acoustic-emission sensor (model SE2MEG-P, Dunegan Engineering Company) is used to detect the occurrence of crack events during the healed-specimen tests. Data from the acoustic-emission sensor are collected with a digital oscilloscope (model LC584A, LeCroy) and then exported to a computer for correlation with the load-time data to determine the load at which the crack reopened. The heal efficiency η is defined as the ratio of the healed fracture toughness to that of the original fracture toughness, which simplifies to a ratio of the fracture loads, calculated as $\eta = P^{Healed}/P^{Original}$ [34]. After fracture, the specimen is fatigued for 50 cycles at 50 μm s^{-1}, with crosshead amplitude of 100 μm (≈20 N) and R-ratio of 0.17 ± 0.04. An amplitude of 100 μm is deemed optimal based on visual observation of the fluid within the crack plane. Between testing cycles, specimens are held at 30 °C for 48 h to cure material in the crack plane under controlled temperature conditions.

Acknowledgements

The authors gratefully acknowledge funding for this project provided by AFOSR Multidisciplinary University Research Initiative (Grant # FA9550-05-1-0346). C. Hansen is supported in part by an NSF Graduate Student Fellowship. K. Toohey was supported in part by the Beckman Institute for Advanced Science and Technology Graduate Fellows Program. Supporting Information is available online from Wiley InterScience or from the author.

Received: February 18, 2009
Revised: April 29, 2009
Published online:

[1] G. B. West, J. H. Brown, B. J. Enquist, *Nature* **1999**, *400*, 664.
[2] A. Roth-Nebelsick, D. Uhl, V. Mosbrugger, H. Kerp, *Ann. Botany* **2001**, *87*, 553.
[3] N. M. Holbrook, M. A. Zwieniecki, *Vascular Transport in Plants*, Elsevier Academic Press, Burlington, MA **2005**.
[4] L. Sack, K. Frole, *Ecology* **2006**, *87*, 483.
[5] G. B. West, J. H. Brown, B. J. Enquist, *Science* **1997**, *276*, 122.
[6] B. Sapoval, M. Filoche, E. R. Weibel, *Proc. Natl. Acad. Sci. USA* **2002**, *99*, 10411.
[7] R. K. Jain, *Science* **2005**, *307*, 58.
[8] N. W. Choi, M. Cabodi, B. Held, J. P. Gleghorn, L. J. Bonassar, A. D. Stroock, *Nat. Mater.* **2007**, *6*, 908.
[9] M. K. Runyon, B. L. Johnson-Kerner, C. J. Kastrup, T. G. Van Ha, R. F. Ismagilov, *J. Am. Chem. Soc.* **2007**, *129*, 7014.
[10] J. M. Higgins, D. T. Eddington, S. N. Bhatia, L. Mahadevan, *Proc. Natl. Acad. Sci. USA* **2007**, *104*, 20496.
[11] D. Lim, Y. Kamotani, B. Cho, J. Mazumder, S. Takayama, *Lab Chip* **2003**, *3*, 318.
[12] D. H. Kam, J. Mazumder, *J. Laser Appl.* **2008**, *20*, 185.
[13] D. Therriault, S. R. White, J. A. Lewis, *Nat. Mater.* **2003**, *2*, 265.
[14] K. S. Toohey, N. R. Sottos, J. A. Lewis, J. S. Moore, S. R. White, *Nat. Mater.* **2007**, *6*, 581.
[15] P. Martin, *Science* **1997**, *276*, 75.
[16] E. N. Brown, S. R. White, N. R. Sottos, *Compos. Sci. Technol.* **2005**, *65*, 2474.
[17] R. S. Trask, H. R. Williams, I. P. Bond, *Bioinspiration and Biomimetics* **2007**, *2*, P1.
[18] A. S. Jones, J. D. Rule, J. S. Moore, N. R. Sottos, S. R. White, *J. R. Soc. Interface* **2007**, *4*, 395.
[19] J. P. Youngblood, N. R. Sottos, *MRS Bull.* **2008**, *33*, 732.
[20] D. Therriault, R. F. Shepherd, S. R. White, J. A. Lewis, *Adv. Mater.* **2005**, *17*, 395.
[21] S. R. White, N. R. Sottos, P. H. Geubelle, J. S. Moore, M. R. Kessler, S. R. Sriram, E. N. Brown, S. Viswanathan, *Nature* **2001**, *409*, 794.
[22] K. S. Toohey, C. J. Hansen, J. A. Lewis, S. R. White, N. R. Sottos, *Adv. Funct. Mater.* **2009**, *19*, 1399.
[23] H. R. Williams, R. S. Trask, I. P. Bond, *Smart Mater. Struct.* **2007**, *17*, 1198.
[24] H. R. Williams, R. S. Trask, I. P. Bond, *Compos. Sci. Technol.* **2008**, *68*, 3171.
[25] D. Therriault, S. R. White, J. A. Lewis, *Appl. Rheol.* **2007**, *17*, 10112-1.
[26] E. Hecht, H. Hoffmann, *Langmuir* **1994**, *10*, 86.
[27] G. E. Yu, Y. Deng, S. Dalton, Q. G. Wang, D. Attwood, C. Price, C. Booth, *J. Chem. Soc. Faraday Trans.* **1992**, 2537.
[28] P. Linse, M. Malmsten, *Macromolecules* **1992**, *25*, 5434.
[29] M. Bohorquez, C. Koch, T. Trygstad, N. Pandit, *J. Colloid Interface Sci.* **1999**, *216*, 34.
[30] J. J. Escobar-Chávez, M. López-Cervantes, A. Naïk, Y. N. Kalia, D. Quintanar-Guerrero, A. Ganem-Quintanar, *J. Pharm. Pharm. Sci.* **2006**, *9*, 339.
[31] K. Kato, *J. Jpn. Soc. Mech. Eng.* **1915**, *19*, 41.
[32] J. Ratzersdorfer, *Die Knickfestigkeit von Stäben und Stabwerken*, Springer, Wien, Austria **1936**, Ch. 3.
[33] S. J. Cox, C. M. McCarthy, *Soc. Industrial Appl. Mathematics* **1998**, *29*, 547.
[34] K. S. Toohey, N. R. Sottos, S. R. White, *Exp. Mech*, in press (DOI: 10.1007/S11340-008-9176-7).